PAPER

Tetracycline catalytic photodegradation with mesoporous phosphated TiO$_2$: characterization, process optimization and degradation pathway†

Huayu Yuan,[a] Qi Su,[a] Yuehu Wang, [ID][ab] Jiang Li, [ID]*[abc] Baojun Liu, [ID][a] Yancheng Li[ab] and Pan Wu[ab]

Concern about the effect of tetracycline (TC) on the ecosystem has been increasing due to its endurance and low decomposition. Photocatalysts have attracted extensive interest as alternatives to other ordinary wastewater treatment methods. A nanosized mesoporous phosphated TiO$_2$ (P-TiO$_2$) photocatalyst was fabricated to degrade TC under Xe lamp irradiation. The TC degradation and COD removal rate reached 98.97% and 79.16% within 30 min. Photocatalysts were characterized by SEM, HRTEM, BET, DRS, XRD, XPS and FT-IR techniques. 31 experiments were designed to identify the best conditions for photocatalytic degradation of TC by response surface methodology (RSM) based on a central composite design (CCD). 6 key operating parameters were selected to study their interrelationships by CCD design. Based on the experimental data and ANOVA, the coefficient of determination (R^2), the values of "Prob > F" and F-value were determined to be 0.9692, 0.002 and 7.87, respectively, which demonstrated that the model is significant. And the excellent correlation between the predicted and actual values also provided good confidence in the model. To achieve a higher removal rate of TC under appropriate and more economical experimental conditions, the optimum values of P-loading on TiO$_2$, concentration of P-TiO$_2$, irradiation time, photo intensity, pH and concentration of TC should be set to 17.45 wt%, 1.00 g L^{-1}, 40.39 min, 5 A, 7, 29.93 mg L^{-1}, respectively, in which the degradation of TC can reach 99.16%. Furthermore, the intermediates of TC verified by GC-MS analysis were mainly chains and rings. A possible pathway of photodegradation was also proposed.

[a]College of Resources and Environmental Engineering, Guizhou University, 550025, Guiyang, Guizhou, China. E-mail: jli82@gzu.edu.cn

[b]Guizhou Karst Environmental Ecosystems Observation and Research Station, Ministry of Education, 550025, P. R. China

[c]College of Chemical and Biological Engineering, Zhejiang University, 310058, Hangzhou, Zhejiang, P. R. China

† Electronic supplementary information (ESI) available. See DOI: 10.1039/d1ra00516b

1 Introduction

Antibiotics produced by bacteria, mold or other microorganisms are a class of secondary metabolites with anti-pathogenic activity.[1] TC is an important antibiotic that is used to treat diseases caused by various bacteria in humans and animals.[2,3] China is the largest antibiotic user in the world, producing approximately 210 000 tons of antibiotics annually, of which 42% were used for medical treatment.[4] With the rapid development of livestock, only 10–20% of antibiotics are metabolized by organisms. However the unmetabolized parts are directly or indirectly discharged into the water environment.[5] Traditional sewage treatment technologies cannot completely remove these residual antibiotics. Due to the persistence and decomposition ability of TC, there are increasing concerns about the impact on ecosystems.[6,7]

In recent years, advanced oxidation processes (AOPs) have become an ideal method of antibiotic degradation due to their advantages of high efficiency, low cost and environmental-friendly.[8] In particular, photocatalysts are considered as alternatives to other traditional wastewater treatment methods because of strong oxidation ability of active radicals ('OH and 'O$_2^-$ *etc.*), which can oxidize large refractory organic molecules into low-toxicity or nontoxic small molecules.[9] Finally it can realize antibiotic removal and mineralization,[10] providing a new treatment method for the harm-free treatment of antibiotics in wastewater. However the fast recombination rate of photo-generated electron–hole (e$^-$/h$^+$) pairs is a major disadvantage in photocatalytic processes.[11] Loading and doping photocatalysis with elements is an effective way to reduce the recombination rate.[12] Meanwhile the specific surface area and particle size are improved to enhance the photocatalytic activity in the process.[13]

Semiconductors based on TiO$_2$ have come to be the most common photocatalysts used in the treatment of pollutants due to their excellent catalytic performance, good stability and low cost.[14–17] However, the catalytic performance of these semiconductors depended largely on the photogenerated electron–

hole pair migration and adsorption on the surface for pollutants.[18] In other studies, P-TiO$_2$ was used for the conversion of glucose to a chemical raw material in photo (5-hydroxymethylfurfural).[19] It had been proven that the interaction between TiO$_2$ and phosphate was helpful for increasing the photocatalytic activity due to the adsorption and photocatalytic capacity of P-TiO$_2$. The results of our pilot study showed that P-TiO$_2$ is very effective in degradation the antibiotic TC. However, the factors that affect the TC removal still need to be further studied with a scientific method for estimating the effectiveness of this method. Response surface methodology (RSM) is used to design experiments for evaluating the impact of multiple factors and obtaining the best conditions in a limited number of planned experiments based on statistical and mathematical methods.[20] Central composite design (CCD) is the most frequently selected method in the RSM technique.[21] Using the RSM to optimize influential parameters has been reported for several optimizations of the pollutant removal process.[22,23]

Herein, P-TiO$_2$, a promising candidate, was fabricated to absorb and photodegrade TC *via* a neutral amine sol–gel technique in this study. Then, RSM was used to optimize six process parameters (concentration of P-TiO$_2$ and TC, irradiation time, P-loading on TiO$_2$, photo intensity and solution pH). The feasibility of the photocatalysis system for TC removal was evaluated under optimized conditions. The intermediates of photodegradation were analyzed by gas chromatography-mass spectrometry (GC-MS). Furthermore the possible pathway of photodegradation was discussed.

2   Materials and methods

2.1   Fabrication and characterization of P-TiO$_2$

TC (M_w: 480.9, purity 98%) was purchased from J&K SCIENTIFIC LTD. Titanium(IV) butoxide (purity 99%), ammonium hydroxide, *n*-butanol, H$_2$SO$_4$ and ammonium phosphate monobasic were obtained from Tian in Fuyu Fine Chemical Co., Ltd. All solutions were prepared with a conductivity of 18 MW cm^{-1}. P-TiO$_2$ was fabricated according to the following literature method.[19] Titanium hydroxide hydrate was prepared by the neutral amine sol–gel technique using *n*-butyl titanate as the TiO$_2$ precursor.

(1) The alkoxide precursor (*n*-butyl titanate, 1–2 drops per min) was added dropwise to n-butanol solution (300 mL) with stirring (1000 rpm) to prepare a milky sol. The mass of *n*-butyl titanate is approximately 21.18 g.

(2) The solution pH was adjusted to be neutral (pH = 7) by adding ammonia before stirring in 12 h for getting the gelation.

(3) After gelation, a rotary evaporator (90 °C, 2 h) was used to remove excess solvent. And then the sample was dried at 80 °C for 12 h to obtain dry titanium hydroxide hydrate.

(4) Phosphated TiO$_2$ was prepared by impregnating titanium hydroxide hydrate with the different amount of ammonium dihydrogen phosphate aqueous solution. To load *x*wt% phosphate (*x*P-TiO$_2$) on TiO$_2$, the dried hydrated TiO$_2$ was added to the dissolving phosphate precursor in water. After stirring at room temperature for 4 h, P-TiO$_2$ was dried at 80 °C for 12 h to evaporate excess water.

(5) After calcination at 550 °C for 4 h, the pure phosphide TiO$_2$ was obtained.

Catalyst samples were specified as *x*P-TiO$_2$, where *x* is 0.76 wt%, 5 wt%, 12.5 wt%, 20 wt% and 24.24 wt%. The addition of 0.76P, 5P, 12.5P, 20P and 24.24P to TiO$_2$ was carried out though using the same procedure but with different phosphate contents. A Bruker D8 diffractometer with Cu-Kα radiation was used to analyze the functional group and crystal structure information of P-TiO$_2$ contained in X-ray diffraction analysis (XRD, $\lambda = 0.15406$ nm, 45 kV, 40 mA). The morphologies were characterized by scanning electron microscopy (SEM, JSM-6701F, JEOL, Carbon tape, Japan) at 5 kV and transmission electron microscopy (TEM, JEM-2100F, Hitachi, Japan). And X-ray photoelectron spectroscopy was used to confirm whether the P was loaded on TiO$_2$ (XPS, ESCALAB 250Xi, ThermoFisher Ltd., USA). The XPS measurements were carried out in an ultrahigh vacuum system in which the base pressure in both chambers was 1×10^{-8} mbar. KBr-pressed pellets were used to characterize the P-loaded TiO$_2$ photocatalast by FTIR. Spectra were recorded from 7800 to 350 cm^{-1} on a Vertex 70 FTIR spectrometer (Bruker Optics Inc., Billerica, MA). The spectral resolution was 0.5 cm^{-1}.

The specific surface area was calculated using the Brunauer–Emmett–Teller (BET, 3H-2000PS2, China) method on the adsorption date in the relative pressure range of 0.07–0.31. The total pore volumes were estimated from the adsorbed amount at a relative pressure of $P/P_0 = 0.98$. Nitrogen adsorption–desorption isotherms of the catalyst were evaluated at −195.8 °C on a Quantachrome Instruments (Autosorb iQ Station 1) sorption analyzer. Before the measurement, the sample was outgassed at 120 °C under vacuum (6.58×10^{-5} torr) for 18.5 h. The Design Expert Version 8.0.6 software package was used to design the experiments.

The photoelectron chemical measurements were all performed in a quartz cell of a three-electrode electrochemical system (CHI-660E, China). The reference electrode is the silver–silver chloride electrode (Ag/AgCl), and the counter electrode is the platinum wire. The working electrode is the carbon cloth (2 × 2 cm^2) coated photocatalyst (5 mg mL^{-1}). The electrolyte is Na$_2$SO$_4$ solution (0.1 M). A Xe lamp was used as the light source, after keeping in the dark for 200 seconds to get a steady dark current.

2.2   Photocatalytic activity

A Xe lamp (YM-GHX-XE-300) was used to simulate the irradiation of solar light. A small mass of the prepared catalyst was put into a lightproof stainless steel container with different concentrations TC (50 mL). The *x*P-TiO$_2$ catalyst was dispersed by an ultrasound instrument for 10 min to ensure the adsorption–desorption equilibrium, and then the solution stirred magnetically for 30 min in the dark before irradiation. The photodegraded TC samples were collected in brown vials at a design interval time, which concentrations of TC were measured by LC-MS (LC: Agilent Technologies 1290 Infinity; MS: AB SCIEX QTRAP 6470, USA Agilent Inc.). Chemical Oxygen Demand (COD) measured by DR1010 (USA HACH Inc.) can

prove the TC degradation after photocatalytic. The TC degree removal was determined based on eqn (1).

$$Y = \left(1 - \frac{C_t}{C_0}\right) \times 100\% \qquad (1)$$

where Y is the degradation rate of TC; C_t (mg L^{-1}) is the concentration of TC at irradiation time "t"; C_0 (mg L^{-1}) is the initial concentration. In this study; The concentrations (C_0 and C_t) imported into The Design Expert Version 8.0.6 for statistical analysis was limited in range (5–32), in order to avoid errors caused by environmental factors (natural light, temperature, solubility, expiration date, *etc.*) for TC stock solution.

2.3 Statistical modeling and analysis

The nonlinear multivariable regression was used to model the experimental data. The experimental data was modeled by eqn (2).

$$y = b_0 + \sum_{i=1}^{n} b_i x_i + \sum_{i=1}^{n} b_{ii} x_i^2 \sum_{i=1}^{n-1} \sum_{j=i+1}^{n} b_{ij} x_{ij} + e \qquad (2)$$

In eqn (2), y is a dependent variable (TC degradation rate); x_i and x_j represent the independent variables photo intensity (A), irradiation time (min), P-loading (wt%), photocatalyst concentration (g L^{-1}), antibiotic concentration (mg L^{-1}) and pH. The regression coefficients (intercept term, linear, quadratic and interaction) in this model are represented by b_0, b_i, b_{ii} and b_{ij}; The e is the error of the model. A smaller P-value (<0.05) and larger F-value indicate the significance of model or parameter.[24] To assess the effect of process variables on TC degradation in this study, a systematic study according to CCD design involving 31 experiments was tested. The range of variables was selected to conduct experiments based on our preliminary and other similar works,[24,25] which was coded as -1 (low) and $+1$ (high) shown in Table 1.

2.4 Analysis of intermediates

Gas chromatography-mass spectrometry (GC-MS, Agilent 7890B with 5975A mass spectrometry, USA) was used to identify and analyze the intermediates. The initial temperature of the column oven was set at 90 °C, which was maintained for 1.8 min; then, the temperature of the column oven went

through three stages: stage 1: increasing up to 180 °C at a rate of 25 °C min^{-1} and holding for 1 min; stage 2: increasing up to 280 °C at a rate of 8 °C min^{-1} and holding for 8 min; stage 3: increasing up to 300 °C at a rate of 20 °C min^{-1} and holding for 0.5 min. The injector temperature was 250 °C. The injection volume was 1.0 μL. And the carrier gas used in this study was helium. Before the analysis, the pH of the sample was adjusted to approximately 4 or 10 by adding 10% H$_2$SO$_4$ or ammonium hydroxide solution dropwise. The solution was extracted with 20 mL of dichloromethane three times. Finally dichloromethane was concentrated to 1.0 mL by rotary evaporation.

3 Results and discussion

3.1 SEM and TEM analyses

The morphologies and the microstructure of P-TiO$_2$ were seen in Fig. 1. The SEM images of 12.5P-TiO$_2$ showed a plate-like morphology marked with blue in Fig. 1a and b. Fig. 1c showed the microstructure of the 12.5P-TiO$_2$ with particle size ranging mostly from 7.87–13.74 nm estimated by Nano Measurer. The high-resolution TEM (HRTEM) image showed a clear lattice spacing of 0.354 nm in Fig. 1d, which is assigned to the (101) plane of anatase TiO$_2$. Comparing with pure TiO$_2$ (P25, 21 nm, Germany), the particle size of as-prepared samples reduced significantly due to phosphate loading on TiO$_2$. And then it formed tiny nano-crystalline clusters. Furthermore, the HRTEM images showed very clear lattice spacing (101), which indicated that the structure of TiO$_2$ was retained after phosphating treatment. The elemental mapping images in Fig. 1e–h indicated that Ti, P and O elements distributed homogeneously within TiO$_2$. These results demonstrated indirectly that element

Fig. 1 (a) and (b) SEM images of P-TiO$_2$; (c) and (d) TEM and HRTEM images of P-TiO$_2$; (e–h) mapping images.

Table 1 Ranges and levels of independent variables for antibiotic removal

Independent variables (code)	Units	Level −1	0	1
Photo intensity (A)	A	10	15	20
Irradiation time (B)	min	40	110	180
P-loading (C)	wt%	5	12.25	20
Photocatalyst concentration (D)	g L^{-1}	1	2.5	4
Antibiotic concentration (E)	mg L^{-1}	5	13.5	32
pH (F)	—	4	7	10

phosphate was uniformly loaded on TiO_2, which was consistent with the results of XRD and XPS scanning analysis.

3.2 XPS analysis

The surface chemical composition of $5P-TiO_2$ were investigated by X-ray photoelectron spectroscopy (XPS). As shown in Fig. 2a, the presence of phosphorus, titanium and oxygen were proved by the signals in the survey XPS spectrum. In addition, no other elements peaks appeared in survey XPS spectrum, implying that $P-TiO_2$ was mainly composed of phosphorus, titanium and oxygen. The peaks of Ti $2p_{3/2}$ and Ti $2p_{1/2}$ shown in Fig. 2b were located at 458.6 and 464.4 eV, respectively, indicating that the oxidation state of the cation is Ti(IV) with an octahedral environment.[26] The high-resolution P 2p spectra shown in Fig. 2c revealed a single peak at 133.4 eV, which showed that the phosphorus loaded on TiO_2 existed in the pentavalent-oxidation state (P^{5+}).[27]

The O 1s peak is located at 529.8 and 531.1 eV in the Fig. 2d, which was assigned to the O–Ti bond in the lattice oxygen of TiO_2 and surface –OH groups.[28] In the Table S1† of $5P-TiO_2$ XPS results, the date showed that phosphorus accounts for 4.55% of the total amount, which was close to the calculated value of 5%. The presence of the C and N elements was due to adhesion from the air to the surface of the material during transportation and testing. The BET and XRD results showed that both specific surface area and crystal size of $P-TiO_2$ have changed because of the loading of phosphorus. Presumably, it may be caused by the formation of Ti–O–P bond. The XPS proved that phosphorus had successfully loaded on TiO_2.

3.3 XRD analysis

The XRD patterns of TiO_2 with different phosphate content (0, 0.76, 5, 12.5, 20 wt%) were shown in the Fig. 3. Comparing the diffraction patterns of all samples with the standard card of TiO_2 anatase phase (JCPDS no. 21-1272) labeled black, it can be seen that they were compatible. In addition, some other peaks that do not belong to the anatase phase of TiO_2 can be seen in the XRD images. After comparative analysis with the database in Jade 6.0 software, it is concluded that these peaks belong to the rutile TiO_2 (JCPDS no. 21-1276) labeled brown. It can be found
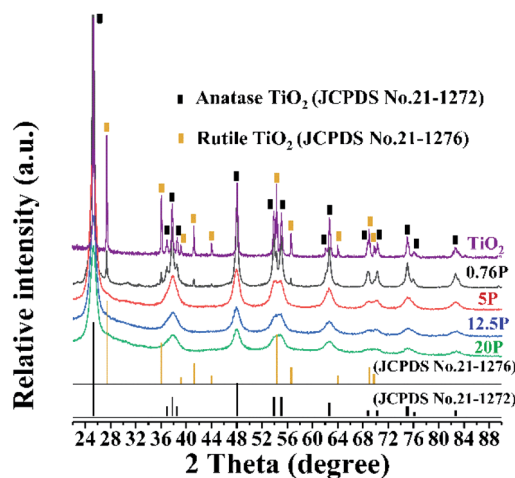

Fig. 3 XRD patterns of (a) $0.76P-TiO_2$, (b) $5P-TiO_2$, (c) $12.5P-TiO_2$ and (d) $20.24P-TiO_2$.
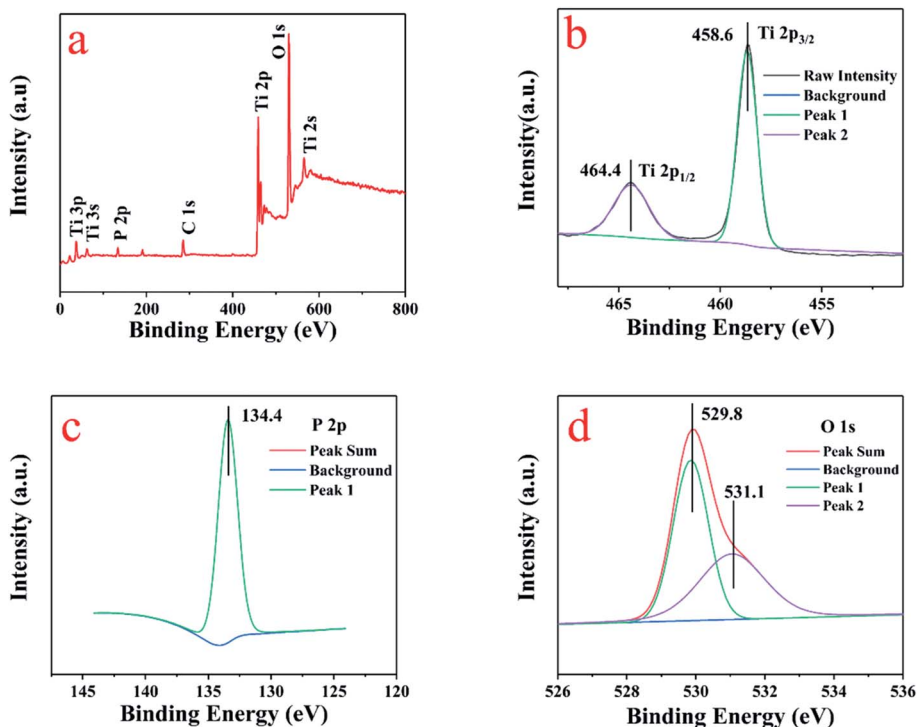

Fig. 2 XPS survey of (a) wide scan; high-resolution spectra (b) Ti 2p; (c) P 2p and (d) O 1s.
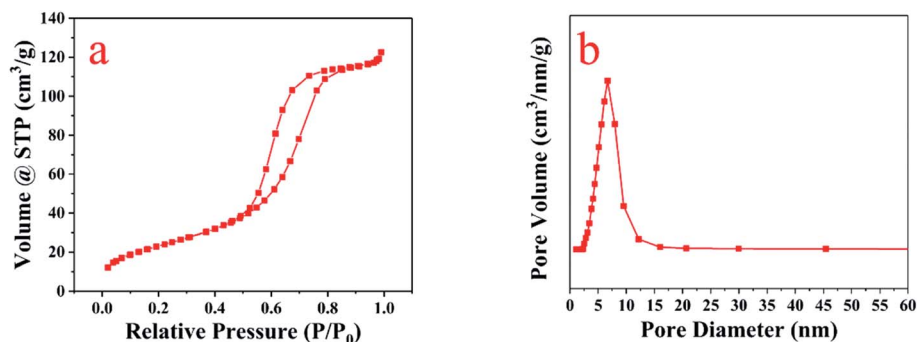
Fig. 4   (a) BET isotherms type and (b) pore size distribution of 12.5P-TiO$_2$.

that the heterojunction of anatase and rutile phase formed after calcination at 550 °C. However, with the increase of phosphorus content in the sample, the characteristic peak of rutile TiO$_2$ disappeared. The diffraction pattern of TiO$_2$ was sharp and intense, which indicated that fabricating TiO$_2$ by the neutral amine sol–gel technique had the high crystallinity. According to the comparison with different phosphorus content samples, the phenomenon of peak broadening and peak intensity reduction appeared after phosphating treatment. It can be concluded that the crystallinity of P-TiO$_2$ particles decreased. Those results indicated that phosphorus had been loaded on TiO$_2$, which was consistent with the results of XPS analysis. Furthermore, according to Debye–Scherrer equation, the crystal size (101) of samples with 0.76–20.24 wt% was between 14.503 and

6.083 nm. An increase in phosphate content resulted in a decrease in the crystal size of the P-TiO$_2$.

3.4   BET analysis

As shown in Fig. 4, the N$_2$ adsorption–desorption isotherm of 12.5P-TiO$_2$ was a type IV isotherm that has a characteristic capillary coagulation step. Comparing with the parameters of pure TiO$_2$ prepared in the same way, the specific surface area (S_{BET}) of the 12.5P-TiO$_2$ sample was increased by about 8 times from 10.4 to 86.514 m^2 g^{-1} (multi point BET). The pore size ranging from 8.0 to 5.2 nm (BJH) and the lower initial pressure of the mesoporous filling stage showed that P-TiO$_2$ promoted the formation of mesoporous structure due to the loading of phosphorus on TiO$_2$. And the phosphate anion played
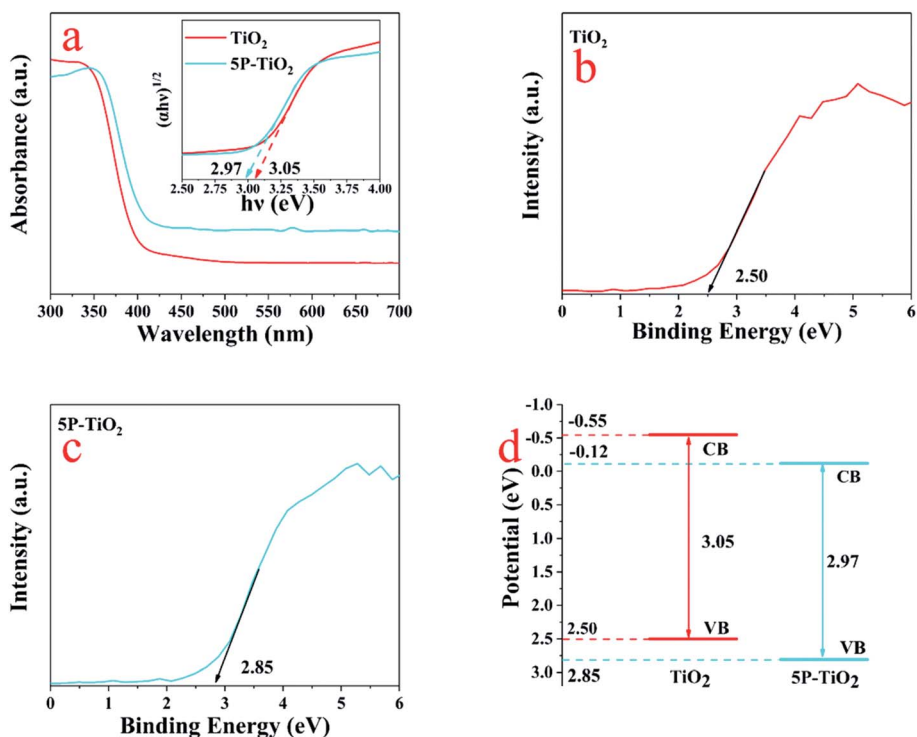

Fig. 5   (a) UV-vis diffused absorption spectra TiO$_2$ and 5P-TiO$_2$; valence-band XPS spectra of (b) TiO$_2$ and (c) 5P-TiO$_2$; (d) band structure diagrams of TiO$_2$ and 5P-TiO$_2$.
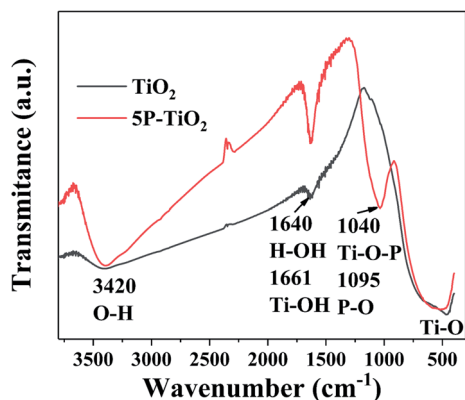
Fig. 6 FTIR spectra of TiO$_2$ and 5P-TiO$_2$.

a stabilizing role in the sintering process. In the process of impregnating dried titanium hydroxide hydrate with ammonium dihydrogen phosphate, the phosphate anions may replace the hydroxyl bridges, which led to the formation of Ti–O–P bonds during calcination. Dalai *et al.* also reported a similar phenomenon in which sulfate ions incorporated into TiO$_2$ delayed the occurrence of sintering.[29]

3.5 The DRS and energy band gaps analysis

The optical properties and valence band potentials of the P-TiO$_2$ were explored by UV-vis diffuse reflectance (DRS) and valence XPS. The band gap energy was obtained from the plot of the modified Kubelka–Munk function *versus* the energy of the absorbed light.[30] In Fig. 5a had represented the UV-visible diffuse reflectance and the absorption edges of samples are in the ultraviolet region with a slight slope to the visible region.

The band gaps were estimated to be 2.97 and 3.05 for the 5P-TiO$_2$ and TiO$_2$, respectively. Fig. 5b and c showed the valence bands (VB) maximum of TiO$_2$ and 5P-TiO$_2$ are 2.50 and 2.81 eV, respectively. According to the energy band gaps, the conduction bands (CB) of TiO$_2$ and 5P-TiO$_2$ are −0.55 and −0.12 eV, respectively. The results showed that phosphorus could cause the downward shift of CB and VB levels (Fig. 5d).

3.6 FT-IR analysis

The FTIR spectra of TiO$_2$ and 5P-TiO$_2$ were shown in Fig. 6. There were a wide absorption peak with moderate intensity at 3420 cm^{-1} and a peak at 1640 cm^{-1}, which was caused by the −OH stretching and bending vibrations of chemical adsorbed water and hydroxyl groups.[31] The strong absorption peak at 1661 cm^{-1} was caused by the bending vibration of the Ti–OH association peak, and the absorption peak between 500 cm^{-1} and 800 cm^{-1} was caused by the stretching vibration of the Ti–O bond in the TiO$_2$ crystal and Ti–O–Ti vibration in octahedral environment.[32] The phosphorus loading on TiO$_2$ improved the adsorption capacity. Two additional broad absorption bands at 1040 and 1095 cm^{-1} were observed in 5P-TiO$_2$, suggesting the chemical environment of the phosphorus in the TiO$_2$. These bands were attributed to P–O vibration.[33] The broad peak at 1095 cm^{-1} was characteristic ν_3 vibration of the phosphate ions coordinated with TiO$_2$. The shoulder peak at 1040 cm^{-1} belonged to Ti–O–P framework vibrations.[34] That means that phosphorus would exist possibly in the surface (as bidentate phosphate) and in the lattice forming Ti–O–P bond.[35]

3.7 Photocatalytic performance

The transient photocurrent responses of pure TiO$_2$, 5P-TiO$_2$ and 12.5P-TiO$_2$ photocatalyst under Xe lamp were shown in Fig. 7a,
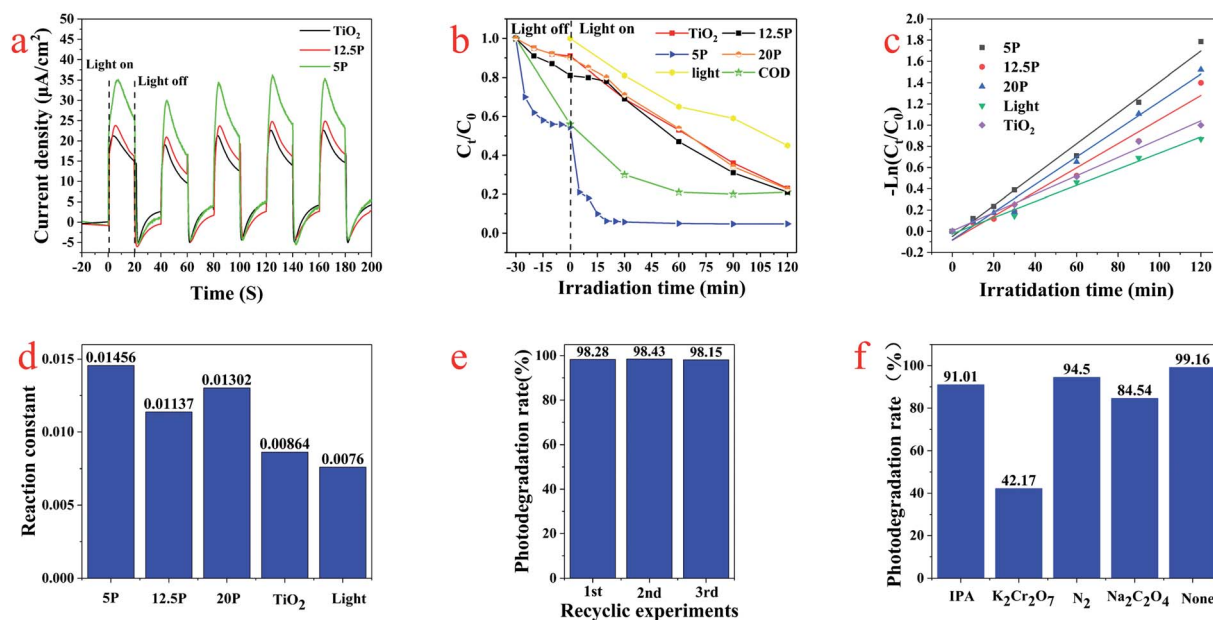

Fig. 7 (a). The transient photocurrent responses of TiO$_2$, 5P-TiO$_2$ and 12.5P-TiO$_2$; (b) photocatalytic degradation of TC by different catalysts and Xe lamp; (c and d) degradation kinetics; (d) and (e) the cycle experiment of 5P-TiO$_2$ photocatalytic degradation for TC; (f) active substance quenching experiment.

which indicated that switching on and off light will lead to change in photocurrent reactions. 5P-TiO$_2$ showed a higher photocurrent response than pure TiO$_2$ and 12.5P–TiO$_2$, which could demonstrate the separation and migration of e$^-$/h$^+$ pair due to phosphorus loading on TiO$_2$. However, 12.5-TiO$_2$ photocatalast with more phosphorus content showed a lower response. Photoelectric experiments proved that the separation efficiency of e$^-$/h$^+$ pair and the carrier migration of photoelectric generation were improved by loading suitable phosphorus on TiO$_2$.

TC was used as the target pollutant to evaluate the photocatalytic performance of the photocatalyst. Fig. 7b showed the adsorption and photocatalytic degradation curves of photocatalysts and pure photolysis for TC. Because the loading of phosphorus led to the smaller particle size and large specific surface area of P-TiO$_2$, the adsorption efficiency of photocatalyst increased from 9.50% (pure TiO$_2$) to 53.68% (5P-TiO$_2$) in darkness without light irradiation. In the photocatalytic degradation process of 120 min, the degradation rates of pure photolysis, pure TiO$_2$, 5P-TiO$_2$, 12.5P-TiO$_2$ and 20P-TiO$_2$ were 58.02%, 85.50%, 99.16%, 85.49% and 85.52%, respectively. In particular, the TC degradation efficiency and COD removal rate reached 98.97% and 79.16% within using 5P-TiO$_2$ as photocatalyst and 30 min under Xe light irradiation, which showed the absorbability and photocatalytic performance of 5P-TiO$_2$ increased significantly compared with pure TiO$_2$. In general, the kinetics of photocatalytic reactions can be explained by quasi-first-order kinetic equations (eqn (3)).

$$-\ln \frac{C_t}{C_0} = kt \tag{3}$$

where, C_0 and C_t are the initial concentration (irradiation time = 0) and the concentration at time t, respectively, and k is the reaction rate constant. In order to study the kinetics of photocatalytic degradation of TC, experiments were carried out under the optimal operating conditions and the initial TC concentration of 30 mg L^{-1}. The photocatalytic degradation kinetics of 5P-TiO$_2$ was compared with that of different photocatalyst and Xe light in the Fig. 7c ($R^2 > 0.97$). The rate constant of 5P-TiO$_2$ was the highest (0.01456 min^{-1}) among them shown in Fig. 7d. The degradation rate constant of 5P-TiO$_2$ was 1.74 and 1.91 times that of TiO$_2$ and Xe light.

The stability of photocatalyst is one of the most important parameters in water treatment process. In order to evaluate the stability of the photocatalyst, the cycle experiment of 5P-TiO$_2$ photocatalytic degradation for TC was carried out under the optimal operating conditions. After each cycle, the photocatalyst was recovered through centrifugation, rinsing and drying for the next cycle. As shown in Fig. 7e, after three cycle experiments, the removal efficiency of 5P-TiO$_2$ for TC remained at 98.0%, which showed that the catalyst had excellent stability.

The active substances in the photocatalytic reaction system including photoinduced hole (h$^+$), photoinduced electrons (e$^-$), hydroxyl radical ($^\bullet$OH) and superoxide radical ($^\bullet$O$_2^-$) may participate in the photocatalytic process. Isopropanol (IPA), potassium dichromate (K$_2$Cr$_2$O$_7$), N$_2$ and sodium oxalate (NaC$_2$O$_4$) were used as scavengers for the active substances $^\bullet$OH,

e$^-$, h$^+$ and $^\bullet$O$_2^-$ to explore the advantageous activity substances produced in the reaction system. In the photodegradation process of TC, the corresponding active substances can be effectively quenched by adding different quenchers, thus reducing the degradation efficiency. As shown in Fig. 7f, the all degradation efficiency of the experiments with quenching agents was reduced comparing with experiment without scavenger (none). Compared with the other three quenching agents, the degradation rate of TC with potassium chromic acid was only 42.17%, indicating that e$^-$ was the active substances mainly involved in photocatalytic reactions system.

3.8 Statistical analysis

In Table S2,† according to the results of 31 experiments, the polynomial function in eqn (4), which can represent the response surface, was used to predict the percentage of TC removal (Y) at the tested parameter values.

$$\begin{aligned}
Y = {} & 88.76102453 + 0.13270485A + 0.21753747B - 1.35794701C \\
& + 2.01540153D + 0.90126905E - 1.21550136F \\
& - 0.01230069AC - 0.35531577AD - 0.08782927AE \\
& - 0.00159106BC + 0.00752543BD - 0.01317150BF \\
& + 0.08021805CD + 0.00978116CE + 0.09986921CF \\
& + 0.16691963DE + 0.15260685DF - 0.05193688EF \\
& + 0.08372494A^2 - 0.00028951B^2 + 0.02297217C^2 \\
& - 0.95483314D^2 - 0.00210221E^2 + 0.12748462F^2
\end{aligned} \tag{4}$$

The significance and adequacy of the model were evaluated by analysis of variance (ANOVA), which provided effective information on the studied parameters, such as the interaction, quadratic and normal linearity.[24] A smaller P-value and a higher F-value for each studied parameters indicated the corresponding coefficient and higher contribution towards the response variable is more significant.[36] In this study, as shown in Table S3,† the F-value (7.87) and P-value (0.0082) imply that the model is adequately significant. More than that, those parameters (B, D, E, AD, AE, BF, CF, DE, EF, A^2, B^2, C^2, D^2 and F^2) were significant model terms because their P-values are less than 0.05. The R^2 (0.9692) of model implies that 96.92% of the variation in the photocatalytic experiment for TC was included, whereas just 3.08% of the variation cannot be accounted for in the studied model. The adjusted R^2 (0.8461) and R^2 (0.9692) values are in reasonable agreement, which confirms the strong relationship between the $Y_{(experimented)}$ and $Y_{(predicted)}$ values in the model. The relationship was also proven in Fig. S2.† The adeq precision value (10.441) represents the signal-to-noise ratio. Generally, a ratio greater than 4 is advantageous for data analysis.

Fig. S1a† showed that nearly all values are near the correlation line, which further confirmed that the model had a considerable accuracy and good reliability between $Y_{(experimented)}$ and $Y_{(predicted)}$. The normal probability plot of the residuals was displayed in Fig. S1b,† which can verify the appropriate standard deviation distribution between $Y_{(experimented)}$ and $Y_{(predicted)}$. The plot showed that there is no extraordinary empirical outputs due to the proximity of residuals around a straight line in this figure. The residual value against the predicted responses showed that the model was

acceptable, as all of the experimental data are within the range of ±3 in Fig. S1c.†[36]

3.9 Response surface analysis of photocatalytic degradation of TC

3.9.1 The influence of variables on the photocatalytic degradation of TC. In order to more intuitively explain the influence of the interaction between variables on the photocatalytic degradation of TC, three-dimensional (3D) graphs and contour graphs with two different independent variables as coordinates were made by Design Expert in Fig. 8. As shown in Fig. 8a, the degradation of TC was up to nearly 100% with a decrease in the concentration of photocatalyst and P-loading, when the other parameters were as follows: photo intensity = 15 A, irradiation time = 90 min, pH = 7 and TC concentration = 17.5 mg L^{-1}. Most likely, the reason for this finding was that the photocatalyst became turbid and saturated, which reduced the light penetration into the suspension.[37,38] In addition, the byproducts of TC and the catalyst particles may compete for the photons emitted from the Xe lamp.[36] However, the interaction between the two was not significant, which was consistent with the results of variance analysis of quadratic polynomial model. In Fig. 8b, TC concentration and photocatalyst concentration showed a similar saddle-shaped surface. When the concentration of TC was low, the TC degradation rate decreased from 97% to 89% with the increase of photocatalyst concentration; when the concentration of TC was high, the removal rate of TC slowly increased to 97.6% with the increase of catalyst concentration

and then gradually stabilized. At the same time, in the case of high catalyst concentration, TC degradation rate showed an uncertain phenomenon, which was caused by agglomeration in the stirring process of high catalyst concentration. As shown in Fig. 8c, there is no obvious interaction between pH and irradiation time. With the increase of irradiation time, the photocatalytic degradation effect was enhanced, which was attributed to the generation of more active substances with the increase of irradiation time. Furthermore, the surface charge of the catalyst, the dissociation of the substrate, contaminant and the electrochemical potential of the photocatalyst may affect it.[39] In Fig. 8d, the intensity of Xe lamp had a greater impact than the irradiation time on photocatalytic degradation. From low intensity to high intensity, the degradation efficiency rises from 86% to 98%, which could be to the higher generation of e$^-$/h$^+$.

As can be seen from Fig. 8 and Table S3,† the significance of the influence of various factors was as follows: irradiation time (*B*, *P*-value = 0.0010) > photocatalyst concentration (*D*, *P*-value = 0.0040) > antibiotic concentration (*E*, *P*-value = 0.0128) > P-loading (*C*, *P*-value = 0.5248) > pH (*F*, *P*-value = 0.5451) > photo intensity (*A*, *P*-value = 0.7129).

3.9.2 Experimental factor optimization and validation. 3D diagrams, an effective way to study the effect of different variables, showed the effect of the process variables studied on TC degradation in Fig. 8. According to the above analysis, the six factors were not only simple monotone function relationship, but also had an optimal ratio group among them so as to achieve the highest TC photodegradation. The experimental results
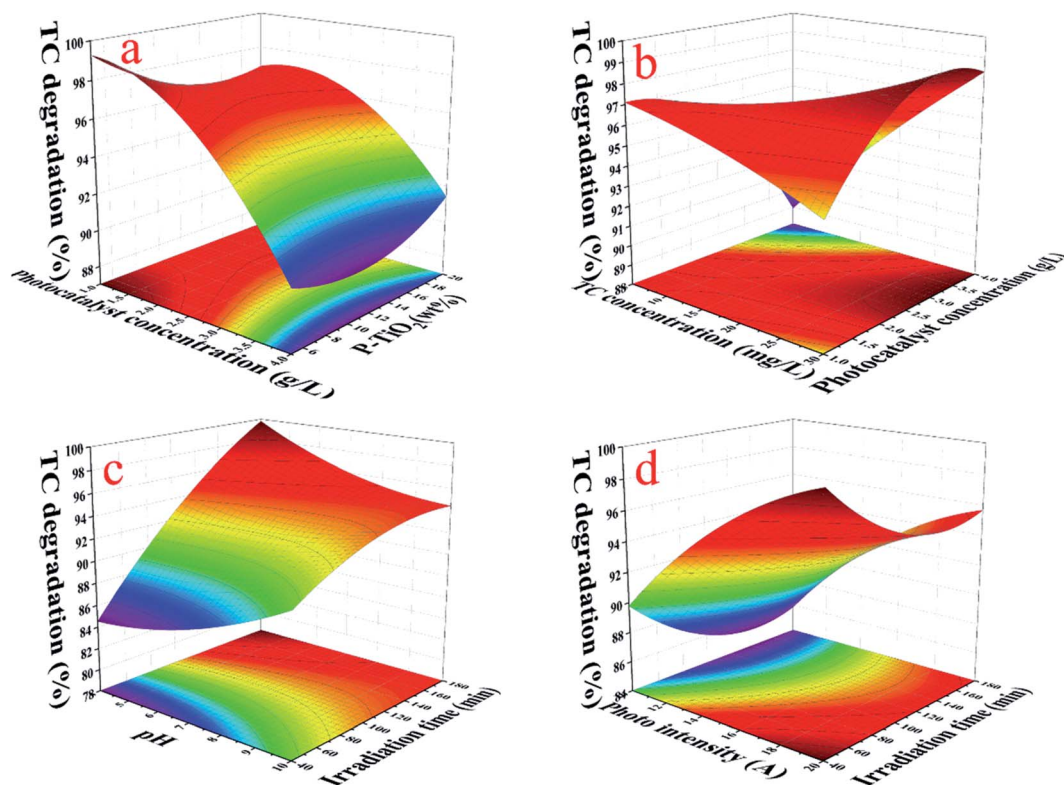

Fig. 8 The three-dimensional (3D) response surface plot of (a) photocatalyst concentration and P-loading on TiO$_2$; (b) photocatalyst concentration and TC concentration; (c) solution pH and irradiation time; (d) photointensity and irradiation time.
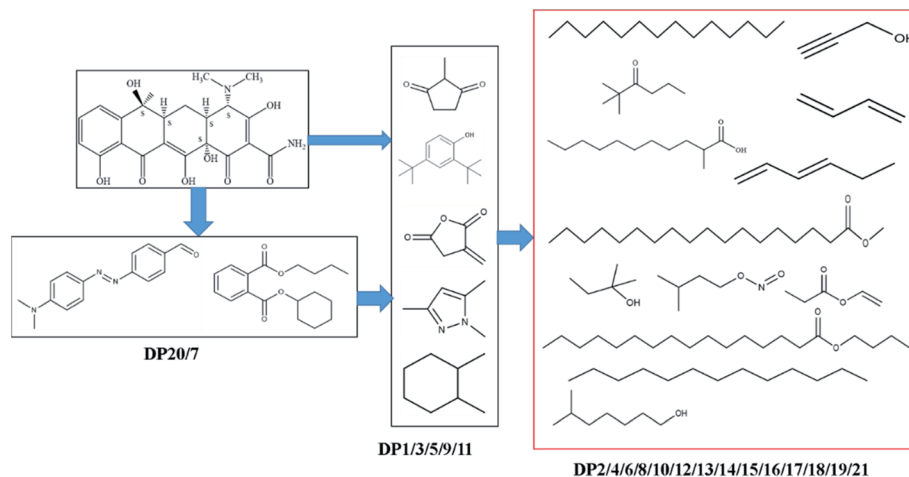
Fig. 9 The proposed removal pathways of photodegradation for TC.

showed that the prepared catalyst had a perfect degradation for TC. Therefore, on this basis, the main purpose of factors optimization was to calculate a more economical and efficient conditions. The method aimed to select the minimum value of photo intensity, irradiation time and catalyst concentration, the appropriate amount of loading on TiO_2, neutral pH (pH = 7), the maximum antibiotic concentration and the best degradation effect by the optimal analysis program of Design Expert software. As shown in Figs. S2 and S3,† the optimum values were 5 A, 40.39 min, 1.0 g L^{-1}, 17.45 wt% and 29.93 mg L^{-1}. In order to verify the practicability and accuracy of the quadratic polynomial model, a verification experiment was carried out under the optimal conditions. The experimental result was 99.16%, and the deviation from the predicted value was only 0.84%. It proved that the fitting quadratic polynomial model was more accurate and reliable in the analysis of TC photodegradation.

3.10 Identification of intermediates and possible degradation pathways

To further clarify the degradation pathway of TC, GC–MS was used to analyze the nonpolar and polar intermediates of degradation during the photocatalysis process.[40] Fig. S4† shows the information of the total ion chromatograms, and 21 intermediates were analyzed and identified by means of the MS spectrum and checked with the NIST database. These intermediates are shown in Table S4.†

The possible degradation pathways are shown in Fig. 9, as proposed on the basis of the above results and previous studies.[41–43] The results showed that the photodegradation process of TC included reactions such as dehydroxylation, N-demethylation, deamination and ring-opening.[44,45] In this study, e⁻ was found to be the main active substance for photocatalytic degradation of TC through quenching experiments. It generated ·O_2^- and ·OH with O_2, which were involved in the photocatalytic degradation of TC. Jin's[46] research also investigated the photodegradation of TC, concluding that different positions of C were attacked by active radicals (·OH, ·O^{2-})

generated by e⁻/h⁺ to produce intermediate products with different molecular structures, such as ring and short-chain products with different functional groups.[40,44] Finally, these products were further transformed into CO_2, H_2O, or the other degradation products.[47]

In the photocatalytic process, these intermediates were mainly formed by the attack of active radicals produced by photocatalysis for TC, especially the ring and groups. The bridging ring and the positions on the hydroxyl, methyl, triamine and formamide were more vulnerable to be attacked. Therefore, we found that more chain and ring products appeared in the mass spectrogram than other literature reports. The preliminary photodegradation products of TC that lost methyl, amino and hydroxyl groups were not detected. The reason for this difference may be the limitations of GC-MC analysis technology. Such phenomenon had been reported in other studies.[40,46]

4 Conclusions

In this study, based on the above analysis, we can draw the following conclusions: (1) the catalyst prepared by the neutral amine sol–gel technique has a larger specific surface area and a slight slope to the visible region due to the loading of phosphorus (Ti–O–P bond), which has a perfect removal effect on tetracycline (99.16%); (2) e⁻ was the active substances mainly involved in photocatalytic reactions in the reaction system. The recycle experiments showed that the photocatalyst had excellent stability, whose the removal efficiency of 5P-TiO_2 for TC remained at 98%; (3) the catalytic degradation of TC was optimized by using the RSM framework of CCD, as the results of ANOVA showed that the irradiation time and the concentration of photocatalyst were the significant factors affecting the degradation of TC; (4) the optimal conditions were P-TiO_2 = 17.45 wt%, photocatalyst concentration = 1.00 g L^{-1}, irradiation time = 40.39 min, light intensity = 5 A, pH = 7 and TC concentration = 29.93 mg L^{-1}, resulting in a TC degradation of 99.16%; (5) according to the intermediates identified by GC-MS,

more chains and rings products appeared in the mass spectrogram in this study. Meanwhile the possible degradation pathways of TC were proposed.

Author contributions

Conflicts of interest

The authors declare that there are no conflicts to declare.

Acknowledgements

Notes and references

1 H. Wang, Y. Wu, M. Feng, W. Tu, T. Xiao, T. Xiong, H. Ang, X. Yuan and J. W. Chew, *Water Res.*, 2018, **144**, 215–225.

2 J. S. Barbieri, O. Hoffstad and D. J. Margolis, *J. Am. Acad. Dermatol.*, 2016, **75**, 1142.

3 S. Petkovic and W. Hinrichs, *Nat. Chem. Biol.*, 2017, **13**, 694–695.

4 Y. Luo, D. Mao, M. Rysz, Q. Zhou, H. Zhang, L. Xu and P. J. J. Alvarez, *Environ. Sci. Technol.*, 2010, **44**, 7220–7225.

5 M. Qiao, G. Ying, A. C. Singer and Y. Zhu, *Environ. Int.*, 2018, **110**, 160–172.

6 A. Javid, A. Mesdaghinia, S. Nasseri, A. H. Mahvi, M. Alimohammadi and H. Gharibi, *J. Environ. Health Sci. Eng.*, 2016, **14**(4), 1–5.

7 J. Wang, D. Zhi, H. Zhou, X. He and D. Zhang, *Water Res.*, 2018, **137**, 324–334.

8 M. H. de Matos Rodrigues, P. A. Rodrigues De Sousa, K. C. M. Borges, L. D. M. Coelho, R. D. F. Goncalves, M. D. Teodoro, F. V. Da Motta, R. M. Do Nascimento and M. Godinho Junior, *J. Alloy. Compd.*, 2019, **808**, 151711.

9 L. Zhao, J. Deng, P. Sun, J. Liu, Y. Ji, N. Nakada, Z. Qiao, H. Tanaka and Y. Yang, *Sci. Total Environ.*, 2018, **627**, 1253–1263.

10 X. Wen, C. Niu, L. Zhang, C. Liang and G. Zeng, *Appl. Catal., B*, 2018, **221**, 701–714.

11 S. Ahmed, M. G. Rasul, R. Brown and M. A. Hashib, *J. Environ. Manage.*, 2011, **92**, 311–330.

12 W. N. A. Guerra, J. M. T. Santos and L. R. R. De Araujo, *Water Sci. Technol.*, 2012, **66**, 158–164.

13 S. Ahmed, M. G. Rasul, W. N. Martens, R. Brown and M. A. Hashib, *Water, Air, Soil Pollut.*, 2011, **215**, 3–29.

14 R. Fagan, D. E. McCormack, D. D. Dionysiou and S. C. Pillai, *Mater. Sci. Semicond. Process.*, 2016, **42**, 2–14.

15 T. Wu, K. Wang, G. Li, S. Sun, J. Sun and J. Chen, *ACS Appl. Mater. Interfaces*, 2010, **2**, 544–550.

16 Z. Lu, F. Chen, M. He, M. Song, Z. Ma, W. Shi, Y. Yan, J. Lan, F. Li and P. Xiao, *Chem. Eng. J.*, 2014, **249**, 15–26.

17 D. Wu, J. Li, J. Guan, C. Liu, X. Zhao, Z. Zhu, C. Ma, P. Huo, C. Li and Y. Yan, *J. Ind. Eng. Chem.*, 2018, **64**, 206–218.

18 F. Chen, Q. Yang, X. Li, G. Zeng, D. Wang, C. Niu, J. Zhao, H. An, T. Xie and Y. Deng, *Appl. Catal., B*, 2017, **200**, 330–342.

19 L. Atanda, S. Mukundan, A. Shrotri, Q. Ma and J. Beltramini, *Chemcatchem*, 2015, **7**, 781–790.

20 S. Khodadoost, A. Hadi, J. Karimi-Sabet, M. Mehdipourghazi and A. Golzary, *J. Environ. Chem. Eng.*, 2017, **5**, 5369–5380.

21 X. Jin, X. Zhou, P. Sun, S. Lin, W. Cao, Z. Li and W. Liu, *Chemosphere*, 2019, **237**, 124433.

22 J. Zhang, D. Fu, Y. Xu and C. Liu, *J. Environ. Sci.*, 2010, **22**, 1281–1289.

23 M. Samy, M. G. Ibrahim, M. Gar Alalm and M. Fujii, *Sep. Purif. Technol.*, 2020, **235**, 116138.

24 S. Karimifard and M. R. Alavi Moghaddam, *Sci. Total Environ.*, 2018, **640–641**, 772–797.

25 B. Shao, X. Liu, Z. Liu, G. Zeng, Q. Liang, C. Liang, Y. Cheng, W. Zhang, Y. Liu and S. Gong, *Chem. Eng. J.*, 2019, **368**, 730–745.

26 M. Murata, K. Wakino and S. Ikeda, *J. Electron. Spectrosc. Relat. Phenom.*, 1975, **6**, 459–464.

27 S. Guo, S. Han, M. Haifeng, C. Zeng, Y. Sun, B. Chi, J. Pu and J. Li, *Mater. Res. Bull.*, 2013, **48**, 3032–3036.

28 D. Sethi, A. Pal, R. Sakthivel, S. Pandey, T. Dash, T. Das and R. Kumar, *J. Photochem. Photobiol., B*, 2014, **130**, 310–317.

29 A. K. Dalai, R. Sethuraman, S. P. R. Katikaneni and R. O. Idem, *Ind. Eng. Chem. Res.*, 1998, **37**, 3869–3878.

30 Y. Yang, Z. Zeng, C. Zhang, D. Huang, G. Zeng, R. Xiao, C. Lai, C. Zhou, H. Guo, W. Xue, M. Cheng, W. Wang and J. Wang, *Chem. Eng. J.*, 2018, **349**, 808–821.

31 L. Lin, R. Y. Zheng, J. L. Xie, Y. X. Zhu and Y. C. Xie, *Appl. Catal., B*, 2007, **76**, 196–202.

32 J. C. Yu, L. Zhang, Z. Zheng and J. Zhao, *Chem. Mater.*, 2003, **15**, 2280–2286.

33 Y. Xia, Y. Jiang, F. Li, M. Xia, B. Xue and Y. Li, *Appl. Surf. Sci.*, 2014, **289**, 306–315.

34 K. Elghniji, J. Soro, S. Rossignol and M. Ksibi, *J. Taiwan Inst. Chem. Eng.*, 2012, **43**, 132–139.

35 L. Körösi, S. Papp, I. Bertóti and I. Dékány, *Chem. Mater.*, 2007, **19**, 4811–4819.

36 A. Mirzaei, L. Yerushalmi, Z. Chen, F. Haghighat and J. Guo, *Water Res.*, 2018, **132**, 241–251.

37 S. Ding, J. Niu, Y. Bao and L. Hu, *J. Hazard. Mater.*, 2013, **262**, 812–818.

38 M. N. Abellán, J. Giménez and S. Esplugas, Selected papers presented at the 5th European Conference on Solar Chemistry and Photocatalysis: Environmental Applications (SPEA 5), 4-8th October 2008, *Catalysis Today*, 2009, **144**, 131–136.

39 B. Boruah, R. Gupta, J. M. Modak and G. Madras, *J. Photochem. Photobiol., A*, 2019, **373**, 105–115.

40 X. Zhu, Y. Wang, R. Sun and D. Zhou, *Chemosphere*, 2013, **92**, 925–932.

41 J. Cao, Z. Yang, W. Xiong, Y. Zhou, Y. Peng, X. Li, C. Zhou, R. Xu and Y. Zhang, *Chem. Eng. J.*, 2018, **353**, 126–137.

42 Z. Xie, Y. Feng, F. Wang, D. Chen, Q. Zhang, Y. Zeng, W. Lv and G. Liu, *Appl. Catal., B*, 2018, **229**, 96–104.

43 M. Ouyang, X. Li, Q. Xu, Z. Tao, F. Yao, X. Huang, Y. Wu, D. Wang, Q. Yang, Z. Chen and Z. Pi, *J. Colloid Interface Sci.*, 2020, **566**, 33–45.

44 N. Barhoumi, H. Olvera-Vargas, N. Oturan, D. Huguenot, A. Gadri, S. Ammar, E. Brillas and M. A. Oturan, *Appl. Catal., B*, 2017, **209**, 637–647.

45 Y. Deng, L. Tang, G. Zeng, J. Wang, Y. Zhou, J. Wang, J. Tang, L. Wang and C. Feng, *J. Colloid Interface Sci.*, 2018, **509**, 219–234.

46 J. Jin, M. Liu, L. Feng, H. Wang, Y. Wang, T. A. H. Nguyen, Y. Wang, J. Lu, Y. Li and M. Bao, *Sci. Total Environ.*, 2019, **695**, 133694.

47 J. Li, M. Han, Y. Guo, F. Wang, L. Meng, D. Mao, S. Ding and C. Sun, *Appl. Catal., A*, 2016, **524**, 105–114.